Magnetic moment and local magnetic induction of superconducting/ferromagnetic structures subjected to crossed fields: experiments on GdBCO and modelling.

J F Fagnard[1], M Morita[2], S Nariki[2], H Teshima[2], H. Caps[3], B Vanderheyden[1] and P Vanderbemden[1]

[1] University of Liège, Department of Electrical Engineering & Computer science (B28), Sart-Tilman, B-4000 Liège, Belgium
[2] Nippon Steel & Sumitomo Metal Corporation, Shintomi 20-1, Futtsu, Chiba 293-8511, Japan
[3] University of Liège, Physics Department, GRASP (B5), Sart-Tilman, B-4000 Liège, Belgium

E-mail : fagnard@montefiore.ulg.ac.be

Abstract

Recent studies have shown that ferromagnetic materials can be used together with bulk high temperature superconductors in order to improve their magnetic trapped field. Remarkably, it has also been pointed out that ferromagnets can help in reducing the crossed field effect, namely the magnetization decay that is observed under the application of AC transverse magnetic fields. In this work, we pursue a detailed study of the influence of the geometry of the ferromagnetic part on both trapped fields and crossed field effects. The magnetic properties of the hybrid superconducting / soft ferromagnetic structures are characterized by measuring the magnetic moment with a bespoke magnetometer and the local magnetic field density with Hall probes. The results are interpreted by means of 2D and 3D numerical models yielding the distribution of the superconducting currents as a function of the ferromagnet geometry. We examine in details the distortion of the shielding superconducting currents distribution in hybrid structures subjected to crossed magnetic fields. These results confirm the existence of an optimum thickness of the ferromagnet, which depends on the saturation magnetization of the ferromagnetic material and the current density of the superconductor. A hybrid structure providing an efficient protection against the crossed magnetic field while maintaining the magnetic induction along the axis of the structure is suggested. The limitations of the 2D modelling in this configuration are discussed.

I. Introduction

Bulk superconductors have proved their significant potential [1-3] in comparison to traditional permanent magnets in several engineering applications including magnetic bearings, levitation systems or rotating machines [4-8]. Recently, the investigation on the combination of ferromagnetic (FM) and bulk superconducting (SC) materials in macroscopic SC/FM structures was intensively conducted in order to study the influence of the ferromagnet behaviour on the enhancement of the magnetic properties, in particular the trapped flux density [9, 10]. The ferromagnetic part can be a disk placed on the SC sample [9], a surrounding tube [3, 11] or even powder or rods inserted inside holes drilled in the SC pellet [12-14]. In addition to the improvement of the magnetic properties [15, 16], the metallic character

of the FM part can play a beneficial role as mechanical reinforcement [3] or as a heat conductor [14, 17].

Recently, we investigated experimentally the magnetic behaviour of premagnetized hybrid SC/FM structures when they are subjected to cycles of magnetic field applied perpendicularly to their magnetization, in a so-called "crossed field" configuration [18]. In a bulk superconducting trapped field magnet, the trapped field is known to slowly decrease as a temperature dependent logarithmic function of time [19, 20]. In applications (including rotating machines, magnetic bearings or levitation devices), however, the sample can be subjected to a time-varying transverse magnetic field that can be produced by another part of the system. For instance, consider a superconductor pellet which is used as a rotor of a synchronous motor and is supposed to perfectly follow the rotating magnetic field produced by the three-phase stator. In real operation, because of variations of the applied torque of the shaft, the superconductor experiences a variable magnetic field rather than the theoretical constant field of the stator. This causes a lag in the motion of the rotor and a temporary misalignment of the superconductor magnetization with respect to the stator field [21]. Therefore, a magnetic field component transverse to the initial magnetization appears, which may impact this magnetization. It has been shown that when a sample is subjected to cycles of magnetic field applied perpendicularly to their magnetization, in a so-called "crossed field" configuration, this transverse field leads to the collapse of the trapped magnetization. This problem has already been studied by several groups on different materials both theoretically [22-29], and experimentally, either on large samples in a liquid nitrogen bath [30-36] or on smaller samples (~ a few mm^3) at other temperatures [37-40]. In our recent work, we studied experimentally the magnetic behaviour of a large bulk sample (~$1cm^3$) in the crossed field configuration. We showed the beneficial influence of a FM disk placed on the top of a bulk gadolinium barium copper oxide (GdBCO) sample, in the same crossed field configuration, by measuring the local magnetic induction at the centre of the surface opposite the FM disk.

In the present work we aim at studying, both experimentally and numerically, the effect of a FM disk placed in contact with a SC pellet in a crossed field configuration, by analysing not only the local magnetic induction close to the sample but also the magnetic moment of the whole SC/FM structure itself. Magnetic induction measurements are local by definition. So results depends strongly on the location of the sensor and mappings at several elevations are often required to fully characterize a given sample. By contrast, even if the magnetic moment is not a characteristic that is directly exploitable for applications, it is an integral quantity that is an intrinsic characteristic of the sample. Therefore it is important to measure the magnetic moment of such hybrid SC/FM structures as it can give valuable information about the modification of the current distribution inside the sample when the transverse magnetic field is applied. In particular, we examine how evolves the magnetic moment with the FM thickness (i) after magnetization and (ii) during crossed field experiments. We are also interested in knowing if this beneficial effect of the FM layer increases linearly with the thickness of the ferromagnet. This, combined with the local magnetic induction measurements, will help in understanding the crossed field phenomenon.

To reach this goal, a number of experiments are carried out with FM disks of several thicknesses, placed on one or both surfaces of the SC pellet which is subjected to very low frequency (< 1 Hz) transverse magnetic field with amplitudes ranging from 12.5 mT to 200 mT. In addition to these measurements, finite element method (FEM) models in 2D and in 3D are carried out (i) to support the experimental results and, once validated, the model can then be used to extend the range of investigated parameters accessible experimentally and (ii) to bring more information on the nature of the processes at the basis of the demagnetization of the SC pellet and of the protective role of the FM layer against the transverse magnetic field. In particular, we calculate separately the SC and the FM contributions of the magnetic moment and their relative variation with the transverse magnetic field. Then, the penetration of the shielding currents against this transverse field, the possible saturation of the FM layer, and its effect on the SC pellet behaviour are examined as a function of the FM thickness.

Finally we highlight the care that is necessary when analysing the 2D modelling results. We also emphasize the limitation of their generalization to describe the behaviour of a real 3D SC/FM structure. To this aim we study the crossed field configuration for a concentric FM ring placed around a cylindrical SC pellet. This hybrid structure is modelled first by using a 2D approximation of an infinite SC bar with two FM layers on its sides and second by using a true 3D model. We show the differences on the penetration of shielding currents in the superconductor and the saturation of the FM layer.

II. Experiment

The studied superconducting (SC) sample is a GdBCO pellet from Nippon Steel and Sumitomo Metal Corporation (9 mm in diameter and 5 mm in height). The magnetic induction at the surface of the sample at 77 K was measured by Hall probe mapping. The central magnetic induction reaches 200 mT at 77 K.

Soft ferromagnetic (FM) disks ("*Supra50*" from Aperam) of various thicknesses and same diameter as the superconductor are attached on one or both plane surfaces of the SC pellet to build either SC/FM or FM/SC/FM structures. The magnetic properties of this material were characterized previously [9], the saturation magnetization $\mu_0 M_{sat}$ is 1.4 T. In the following, the SC pellet is labelled 0mm (cf. figure 1a), the hybrid structures consisting in the same SC pellet and ferromagnetic disks of 0.35, 0.95, 1.96 and 2.89 mm attached to the top surface are respectively labelled 0.35mm, 1mm, 2mm and 3mm (cf. figure 1b). A last hybrid structure where two 1 mm ferromagnetic disks are attached to the top and the bottom surfaces is labelled 2*1mm (cf. figure 1c).

The axial component of the total magnetic moment of the structures (SC only, SC/FM or FM/SC/FM) is measured at 77 K in a bespoke magnetometer designed to accommodate large bulk samples up to 17 mm in diameter. The specifications and the operations of the experimental system are described in a previous work [41]. The magnetometer is able to measure very large magnetic moments (up to 1 Am²), which is two orders of magnitude above the maximum magnetic moment of commercial cryogenic measurement systems. The samples are first magnetized at 77 K under 0.625 T in a separate electromagnet under field-cooling (FC). Then the time dependence of the magnetic moment is recorded using the magnetometer. The initial magnetic moment m_0 – i. e. when the magnetic field was switched off – is extrapolated from the measurements.

In some experiments, after a given time of 1888 s for the relaxation of the currents (and the trapped field), the sample is subjected to cycles of transverse magnetic field. A ferrite magnetic circuit with two 1200 turn commercial coils and two 400 turn homemade coils is powered by a controlled current source Kepco (50 V - 20 A). The circuit is used to generate the transverse field cycles at low frequency (1 mHz - 10Hz). Amplitudes up to 25 mT can be achieved with our magnetic circuit. Since the waveform would no longer be triangular above 12.5 mT, we choose to limit the maximum applied magnetic induction in the linear range. Twenty groups of 10 cycles of 12.5 mT amplitude at 1 Hz (triangular waveform) are applied to the sample and the magnetic moment is measured every ten cycles.

In order to characterize the crossed field effect at various temperatures below 77 K, a home-made tool is designed for being inserted inside the sample chamber of a 9 T Physical Property Measurement System (PPMS) from Quantum Design. This tool is built with non-magnetic materials (brass, aluminium, copper). It allows a superconducting pellet to be rotated with respect to the direction of the magnetic field generated by the PPMS from a parallel to a perpendicular direction with an accuracy of 0.1°. The tool is designed to sustain a maximal torque of 0.5 Nm. The dimensions of the sample holder are 9 mm in diameter and up to 8 mm in height. A high sensitivity cryogenic Hall probe (Arepoc HHP-VU) and a Pt100 temperature sensor are placed in the sample holder in close contact with the superconductor in order to measure the magnetic flux density at the centre of the sample surface and the local temperature of the sample. The electrical wirings of the sensors are connected to an external dual-channel Agilent 34420A nanovoltmeter through a PPMS blank puck plugged at the bottom of the

sample chamber. The experiments are controlled with a Labview® interface. The sensors signals are acquired alternately on both nanovoltmeter channels. The temperature control is performed by the PPMS system through GPIB commands and using the sample chamber thermometer. The reading of the Pt100 sensor is used to ensure that the thermal stabilization of the sample is achieved before to start any measurement. The magnetic field is also controlled by GPIB commands and the electronics of the PPMS system. The waveform of the applied magnetic field is not a continuous triangular waveform but a succession of "0 – B_{max} – 0" triangular shape at a sweep rate of 0.91 mT/s followed by a dead time of 88 s. Cycles are called "unipolar" when B_{max} is always positive and "bipolar" when B_{max} is alternately positive and negative. This specific waveform was chosen to mimic the procedure used for magnetic moment measurements. A schematic graph of the waveform is displayed in figure 3(c).

III. Modelling

Finite element method (FEM) numerical modelling is carried out using an open-source solver (GetDP) with an A-ϕ formulation in 3D and an A- formulation in 2D. The formulations are described in [42-44]. The constitutive law used to describe the behaviour of the superconductor is an isotropic $E(J)$ power law

$$E(J) = E_c \left(J/J_{c0}\right)^n, \quad (1)$$

where n is the critical exponent and a constant J_{c0} denotes the critical current value at the critical field E_c (1μV/cm). The parameters for modelling the superconducting properties are chosen in order to match as close as possible the magnetic moment measurements and the local magnetic induction measurements on the top surface. A field-independent critical current $J_{c0} = 2.5\ 10^8$ A/m² and the n value of 31 are used in Eq. (1). The FM behaviour is described by the interpolation of the measured $B(H)$ curve displayed in Ref. [9]. We emphasize, however, that care should be taken in interpreting the 3D results because this model neglects potential effects related to longitudinal currents [26].

For the 3D modelling the structure is meshed with tetrahedrons of characteristic length of 500 μm in the SC volume and of 150, 250, or 350 μm in the 1 mm, 2 mm and 3 mm FM layer, respectively. The total number of elements ranges between 76000 and 250000. The calculations are stopped at a fixed residue tolerance, which is set to 10^{-3}. 3D models are the most realistic ones, even though the constitutive law of Eq. (1) ignores potential effects associated with longitudinal currents [45]. Here, 2D models are also considered for two reasons: (i) their geometry can be chosen so that the current density is everywhere perpendicular to the magnetic induction; they are then free from longitudinal current effects; (ii) 2D models are less computationally expensive and can thus be carried out with finer meshes.

For the 2D geometry, we choose an infinite bar with the same cross section as the system. Under an applied magnetic field, currents will be induced in or out the page, perpendicular to the cross section. This geometry can be simulated with less computational effort that the full 3D geometry, while it already captures many aspects of the interaction between the superconductor and the ferromagnet. However, as the induced current flow in or out the page without return loops (or, in other words, the current lines loop 'at infinity'), some of the 3D effects will be neglected. A discussion on the comparison between 3D and 2D approaches will follow in Section V. For the 2D model, the mesh consists of triangles with a characteristic length of 100 μm in the SC part, and either 40 μm or 70 μm in the FM parts (40 μm for the FM layers with a thickness of 0.25 or 0.5 mm, and 70 μm for the layers of thicknesses greater than 1 mm). The number of elements ranges between 40000 and 60000. The less expensive calculations allows one to set a lower residue tolerance, of 10^{-6}. For the flux creep relaxation and for the smallest applied magnetic field, the lower residue tolerance is set to 10^{-10}.

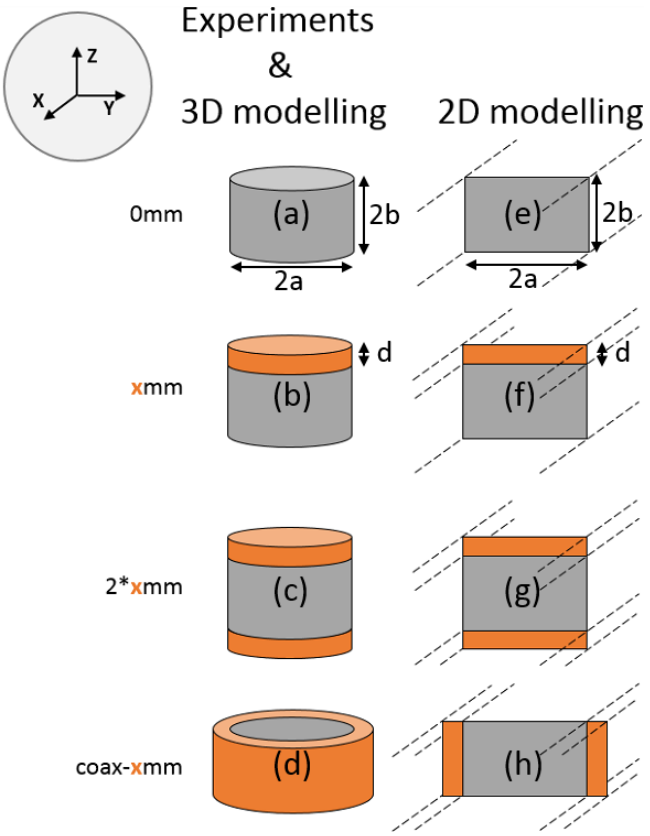

Figure 1: Schematic representations of the studied geometries in experiments (a-c), 3D modelling (a-d) and 2D modelling (e-h). The SC pellet/bar (diameter/width 2*a* and height 2*b*) is labelled 0mm (a and e). The hybrid structures consisting in the same SC pellet/bar and FM disks/bar of several thicknesses (*d* = *x* mm) attached to the top surface are respectively labelled xmm (b and f). The hybrid structure where two FM disks/bars are attached to the top and the bottom surfaces is labelled 2*xmm (c and g). In 3D, the hybrid structure where a FM ring is placed around the SC pellet is labelled coax-xmm (d). In 2D, the hybrid structure where two FM bars are attached to the top and the bottom surfaces of the SC bar is labelled coax-xmm (h).

In both 2D and 3D models, the sample is magnetized along the *z* axis by increasing the magnetic field at a constant rate $\mu_0 \, dH_{app}/dt$ = 15 mT/s up to a maximal value $\mu_0 \, H_{app}$ = 3 T and then decreased to 0 at the same rate. The transverse magnetic field is applied along the *y* axis for 1888 s (the same time as for the trapped field relaxation in experiments) after the end of the magnetization process. We investigated a variety of SC/FM structures; their names are reported in table 1. The structure labelled 0mm (cf. figures 1a and 1e) corresponds to the superconductor alone. The hybrid structures where ferromagnetic disks of 0.25, 0.5, 1, 2 and 3 mm are attached to the top surface of the 0mm sample are respectively labelled 0.25mm, 0.5mm, 1mm, 2mm and 3mm (cf. figures 1b and 1f). A hybrid structure where two 1 mm FM disks are attached to the top and the bottom surfaces is labelled 2*1mm (cf. figures 1c and 1g). Finally, we have studied another SC/FM structure where two FM layers are placed on the sides of the 0mm structure to mimic the behaviour of a FM ring surrounding the SC pellet.

Following the same convention as above, these structures are labelled coax-*x*mm where *x* is the thickness of the FM layer in millimetres (cf. figures 1d and 1h). Notice that even if in 3D the modelled structure is indeed a FM ring around a cylindrical SC pellet (cf. figure 1d), it corresponds to two thin FM bars on the sides of an infinite SC bar in 2D (cf. figure 1h).

The FEM models give us to access to the magnetic induction *B* in the entire modelled space, the current distribution *J* inside the superconductor, the magnetic permeability μ inside the ferromagnetic

material and the magnetic moment contributions of both parts of the hybrid SC/FM structure. The superconducting part of the magnetic moment m_{SC} is calculated from the integral:

$$\vec{m}_{SC} = \frac{1}{2}\int \vec{r} \times \vec{J}\, dV \tag{2}$$

and the ferromagnetic part of the magnetic moment m_{FM} is calculated from the integral:

$$\vec{m}_{FM} = \int \vec{B}(\vec{r}) \left(\frac{1}{\mu_0} - \frac{1}{\mu(\vec{r})}\right) dV. \tag{3}$$

Here we have to point out a difference in the results that can be obtained in 2D and in 3D. In 2D, consider the simple case of a completely penetrated superconducting slab of width 2*a*, height 2*b* and infinite along the *z* axis (cf. figure 1e). In the limit of the Bean model, the *z* component of the magnetic moment per unit length unit is $m_{SC} / \Delta z = J_c\, a^2\, b$. For a fully saturated infinite ferromagnetic slab of width equal to 2*a* and height equal to *d* (cf. figure 1f), the *z* component of the magnetic moment per unit length is equal to $m_{FM} / \Delta z = M_{sat}\, 2a\, d$ where M_{sat} is the saturation magnetization. The ratio of the ferromagnetic magnetic moment over the superconducting magnetic moment is therefore:

$$\frac{m_{FM}}{m_{SC}} = 2\frac{M_{sat}}{J_c}\frac{d}{ab}. \tag{4}$$

The ratio is different in 3D. Consider now the simple case of a completely penetrated superconducting short cylinder of diameter 2*a* and height 2*b* (cf. figure 1a). In the limit of the Bean model, the *z* component of the magnetic moment unit is $m_{SC} = 2\pi/3\, J_c\, a^3\, b$ and that of a fully saturated ferromagnetic disk (cf. figure 1b) of diameter 2*a* and height *d* is given by $m_{FM} = M_{sat}\, \pi\, a^2\, d$. The ratio of the ferromagnetic magnetic moment over the superconducting magnetic moment is therefore:

$$\frac{m_{FM}}{m_{SC}} = \frac{3}{2}\frac{M_{sat}}{J_c}\frac{d}{ab} \tag{5}$$

The comparison of equations (4) and (5) shows that they differ by a factor ¾ which expresses the nature of different demagnetization effects in different geometries. These effects need to be taken into account when comparing the 2D and 3D predictions.

We mention below 4 reference formulae that will be used for the analysis. First, the case of a superconductor obeying the constitutive law given by Eq. (1), the superconducting magnetic moment depends on the ramp rate dB_{app}/dt of the applied field. To take this effect into account corrections were calculated by Brandt in [46] for long (or infinite) bars i.e.

$$m_{SC}/\Delta z = J_c\, a^2\, b\, \left(\frac{dB_{app}/dt}{E_c}a\right)^{1/n} \frac{2n}{2n+1} \tag{6}$$

and for disks

$$m_{SC} = \frac{2\pi}{3}\, J_c\, a^3\, b\, \left(\frac{dB_{app}/dt}{2E_c}a\right)^{1/n} \frac{3n}{3n+1} \tag{7}$$

Second, in the Bean model limit, the analytical expression of the penetration field H_p of the superconducting sample is a function of the geometry. Indeed for an infinitely long bar H_p reads [47]:

$$H_p = \frac{J_c\, b}{\pi}\left[\frac{2a}{b}\arctan\left(\frac{b}{a}\right) + \ln\left(1 + \frac{a^2}{b^2}\right)\right], \tag{8}$$

while for a short cylinder it reads [47-49]:

$$H_p = J_c\, b \ln\left[\frac{a}{b} + \left(1 + \frac{a^2}{b^2}\right)^{1/2}\right]. \tag{9}$$

Table 1: Magnetic moment measurements (m_{EXP}), modelled in 3D (m^{3D}) and in 2D (m^{2D}). The subscripts SC refer to the SC contribution to the modelled magnetic moments. The subscripts FM refer to the FM contribution to the modelled magnetic moments. The subscripts TOT refer to the modelled magnetic moment of the whole hybrid structure by addition of the SC and FM contributions. $m_{TOT}^{2D\ CORR}$ is the addition of the SC contribution and ¾ of the FM contribution of the magnetic moment modelled in 2D. The names of the studied samples are labelled according the nomenclature used in figure 1.

Sample	m_{EXP} (Am²)	m_{SC}^{3D} (Am²)	m_{FM}^{3D} (Am²)	m_{TOT}^{3D} (Am²)	m_{SC}^{2D} (Am)	m_{FM}^{2D} (Am)	$m_{TOT}^{2D}=m_{SC}^{2D}+m_{FM}^{2D}$ (Am)	$m_{TOT}^{2D\ CORR}=m_{SC}^{2D}+¾m_{FM}^{2D}$ (Am)
0mm	0.1169	0.1127	-	0.1127	12.298	-	12.298	12.298
0.25mm	-	-	-	-	12.298	0.358	12.657	12.567
0.35mm	0.1204	-	-	-	12.298	0.499	12.797	12.672
0.5mm	-	0.1125	0.0042	0.1167	12.298	0.707	13.005	12.829
1mm	0.1258	0.1126	0.0083	0.1209	12.298	1.386	13.685	13.338
2mm	0.1340	0.1126	0.0161	0.1287	12.298	2.695	14.994	14.320
3mm	0.1404	0.1125	0.0236	0.1361	12.298	3.971	16.270	15.277
2*1mm	0.1314	0.1125	0.0179	0.1304	12.298	3.046	15.345	14.583
coax-0.25mm	-	-	-	-	12.298	-2.761	9.538	10.228
coax-0.5mm	-	-	-	-	12.298	-5.040	7.258	8.518
coax-1mm	-	0.1126	-0.0487	0.0639	12.298	-7.125	5.174	6.955
coax-2mm	-	-	-	-	12.298	-7.763	4.536	6.476
coax-3mm	-	0.1126	-0.0549	0.0577	12.298	-8.076	4.223	6.242

IV. Results

IV. 1. Magnetic moment after magnetization process: experiments, 2D and 3D modelling

First, the magnetic moment of the hybrid SC/FM structures m_{EXP} is measured with the magnetometer as described above and the respective values are reported in table 1. The magnetic moment for the SC/FM structures is found to increase almost linearly with the FM thickness. Note that the value obtained for the 2*1mm structure which contain two ~1 mm FM disks is very close to that of the 2mm structure. Table 1 also reports the modelled values obtained for the 3D and the 2D geometries and, in particular, the separate contributions of the superconductor and the ferromagnetic parts.

The values of the magnetic moment obtained from the 3D model are found to match the experimental values within a 4% error. It can also be compared to the value calculated in the Bean model limit for a cylinder assuming the parameters values used for modelling. This calculated value, including the Brandt correction by using Eq. (7), is $m_{SC}^{(3D)} = 0.11395$ Am². For an infinite bar, in the Bean model limit, including the Brandt correction by using Eq. (6), we have $m_{SC}^{(2D)} / \Delta z = 12.298$ Am which is the value obtained by 2D modelling. We can attribute the small difference in 3D to the less severe convergence criterion (10^{-3} instead of 10^{-10} for 2D modelling) used in order to save computation time.

In figure 2, we plot the experimental and modelled values of the total magnetic moment normalized to the respective magnetic moment without ferromagnetic layer. We can observe the excellent agreement between the 3D modelling results (open red triangles) and the experimental values (solid black circles). All results exhibit a linear increase of the total magnetic moment with respect to the FM thickness, a result which is expected for a saturated FM layer: its magnetic moment is proportional to the volume of the ferromagnet (and therefore to its height as the diameter is kept constant). However the 2D model seems to overestimate this increase. Nevertheless, if we take into account the considerations discussed in the last section concerning the difference in the ratio m_{FM} / m_{SC} for geometries considered in 2D and 3D we can correct the results in 2D by adding only ¾ m_{FM}^{2D} to m_{SC}^{2D} to obtain the total magnetic moment of the structure $m_{TOT}^{2D\ CORR}$. These corrected values are reported in table 2 and plotted in figure 2. A much better agreement with the experimental data can be observed. For the symmetric 2*1mm hybrid structures a very good agreement between the experiment and both 3D and corrected 2D modelling is also found. For the FM ring (not investigated experimentally)

it is clear that the correction of the 2D modelling values is necessary. The comparison of the normalized magnetic moments reported in table 2 shows that the difference between the corrected 2D modelling and the 3D modelling values drops from 26 % and 33% respectively for a FM thickness of 1 mm and 3 mm to less than 1%. The comparison of this first set of 2D modelling data with the experimental and 3D modelling magnetic moment values draws attention to the fact that 2D modelling values have to be taken with caution when we deal with hybrid SC/FM modelling.

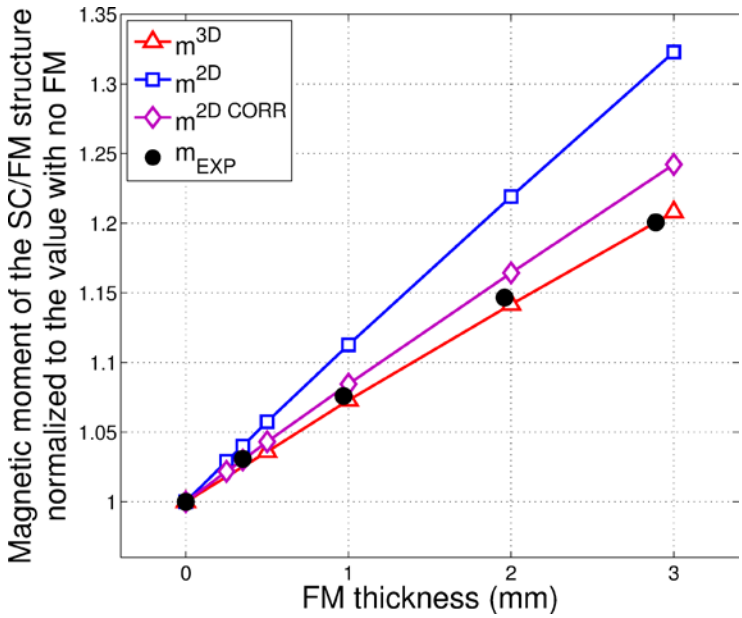

Figure 2: Magnetic moment normalized to the value with no FM: measurements (m_{EXP}), modelled in 3D ($m^{3D} = m_{TOT}{}^{3D}/m_{TOT}{}^{3D}(0mm)$) and in 2D ($m^{2D} = m_{TOT}{}^{2D}/m_{TOT}{}^{2D}(0mm)$) for the whole hybrid structure. In 2D and 3D modelling, it is obtained by addition of the separated SC and FM contributions. The superscript CORR refers to the corrected values obtained by the addition of the SC contribution and ¾ of the FM contribution of the magnetic moment modelled in 2D.

Table 2: Normalized magnetic moment measurements (m_{EXP}), modelled in 3D (m^{3D}) and in 2D (m^{2D}). The subscripts SC refer to the SC contribution to the modelled magnetic moments. The subscripts FM refer to the FM contribution to the modelled magnetic moments. The subscripts TOT refer to the modelled magnetic moment of the whole hybrid structure by addition of the SC and FM contributions. $m_{TOT}{}^{2D\ CORR}$ is the addition of the SC contribution and ¾ of the FM contribution of the magnetic moment modelled in 2D. The names of the studied samples are labelled according the nomenclature used in figure 1.

Sample	m_{EXP} / m_{EXP} (0mm)	$m_{TOT}{}^{3D}$ / $m_{TOT}{}^{3D}$ (0mm)	$m_{TOT}{}^{2D}$ / $m_{TOT}{}^{2D}$ (0mm)	$m_{TOT}{}^{2D\ CORR}$ / $m_{TOT}{}^{2D\ CORR}$ (0mm)
0mm	1	1	1	1
0.25mm	-	-	1.029	1.022
0.35mm	1.0302	-	1.040	1.030
0.5mm	-	1.0355	1.057	1.043
1mm	1.076	1.0728	1.113	1.085
2mm	1.1467	1.142	1.219	1.164
3mm	1.2007	1.2076	1.323	1.242
2*1mm	1.124	1.157	1.248	1.186
coax-0.25mm	-	-	0.776	0.8232
coax-0.5mm	-	-	0.590	0.693
coax-1mm	-	0.567	0.421	0.565
coax-2mm	-	-	0.369	0.527
coax-3mm	-	0.512	0.343	0.508

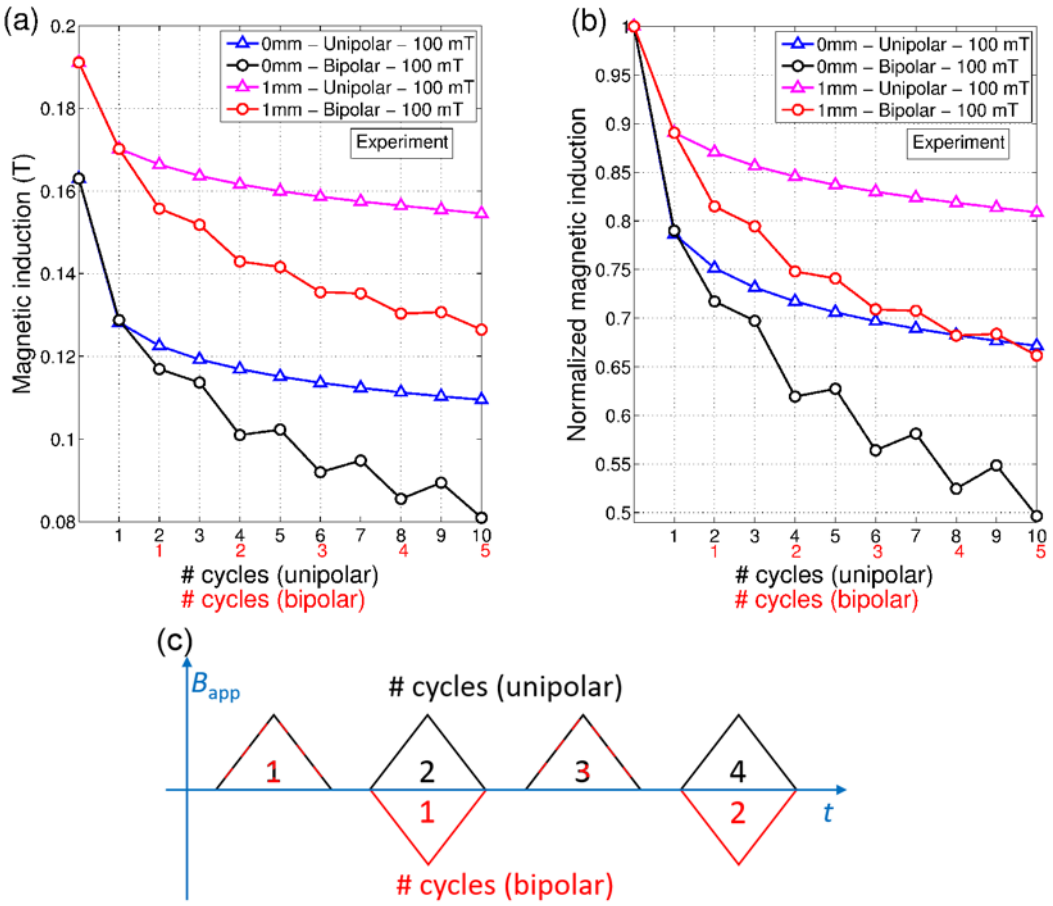

Figure 3: Magnetic induction measured at the bottom surface of the SC pellet (face opposite the FM disk) for 10 cycles of 100 mT unipolar transverse magnetic field (along y axis) and 5 cycles of 100 mT bipolar transverse magnetic field for 0mm and 1mm samples: (a) raw measurements, (b) normalized measurements and (c) schematic graph of the specific waveform used in the experiments.

IV. 2. Measurements of local magnetic induction with Hall probe

Figure 3 shows the experimental results of the magnetic induction measured by the Hall probe at the bottom surface of the SC pellet (face opposite the FM disk) for several cycles of 100 mT transverse magnetic field (along *y* axis) applied at dB_{app}/dt = 0.91 mT/s. We apply either 10 unipolar cycles (i. e. the field is always positive) or 5 bipolar cycles (the field changes its polarity each half-period). A schematic graph of the specific waveform used in the experiments is displayed in figure 3(c). Here, 0mm and 1mm samples are compared.

First, it can be observed that, at the location of the Hall probe, the magnetic induction is found to increase from 163 mT to 191 mT (17 %) in the presence of a 1 mm thick FM disk placed on the opposite side. Unambiguously bipolar cycles have a more detrimental effect on the axial magnetic induction than unipolar cycles for both samples. If we normalize the experimental data to the respective magnetic induction measured just before applying the transverse magnetic field, as presented in figure 3(b), we can also see that the presence of the FM disk leads to smaller decay of the normalized magnetic induction at the location of the Hall probe, as it was already shown in our previous work [18].

The increment of the initial magnetic induction for the 1mm sample with respect to that of the 0mm sample varies along the axis and depends on the FM thickness. Indeed, at a larger distance from the sample, the local value of the magnetic induction can even be smaller with FM disk than without due to the difference in the return line paths. Moreover, the measurement error can be relatively large

due to (i) imprecision in the Hall probe distance from the SC surface, (ii) misalignment with respect to the axis (the transverse field may not be applied exactly at 90°) and (iii) in-field alignment of the sample due to the magnetic torque applied to the sample considering the backlash of the sample holder. The last two sources of error are probably the cause of the ripple that can be seen on the bipolar cases. Indeed a closer look to the measurements within the cycle period shows that the magnetic induction increases slightly during the positive part of the cycle. A very small misalignment coupled to the high J_c anisotropy of the material leads to the appearance of remagnetizing currents which slightly increase the magnetic moment (and therefore the local magnetic induction) when the magnetic field sign changes [50].

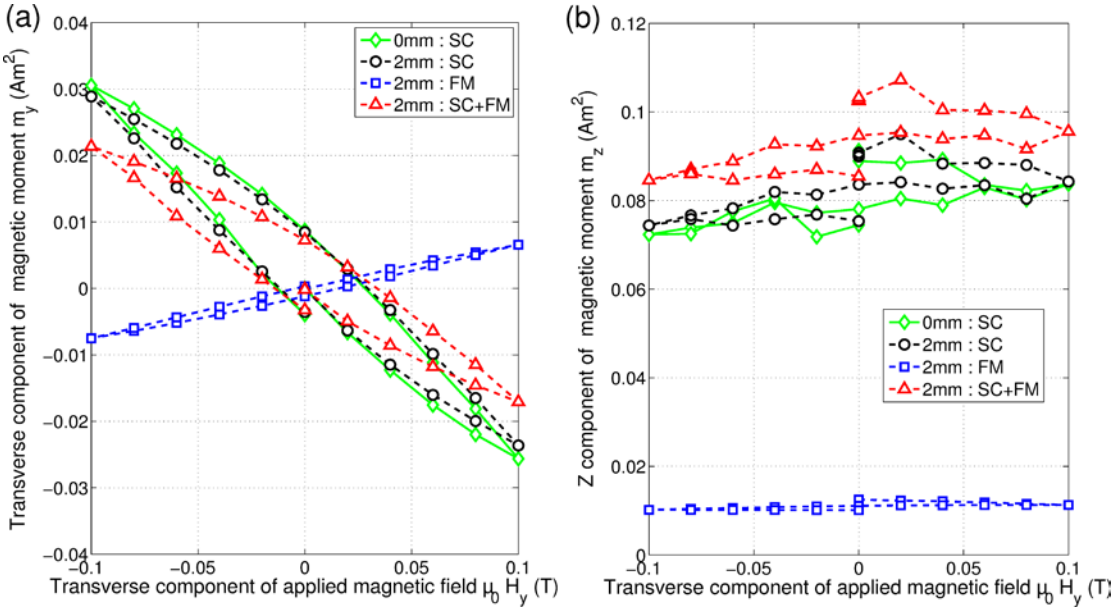

Figure 4: Magnetic moment modelled in 3D for one cycle of 100 mT transverse magnetic field (along y axis) for 0mm and 2mm samples. (a) transverse component of the SC, FM and SC+FM contributions to the magnetic moment m_y, (b) axial component of the SC, FM and SC+FM contributions to the magnetic moment m_z.

IV. 3. 3D modelling of the magnetic moment

We now turn to a 3D model of the magnetic moment of a structure which is first magnetized along the *z* axis and then subjected to a transverse field applied. The transverse field is applied 1888 s after the initial magnetization has ended. It has a strength of 100 mT and is applied for a full cycle. Figure 4 shows the transverse (a) and the axial (b) components of the resulting magnetic moment. The components are split up into the SC and FM contributions. The modelling results are shown for the 0mm and the 2mm samples. During the 1888 s time interval, the magnetic moment m_z was reduced because of the flux creep, from 0.1127 Am² (cf. table 1) to 0.0908 Am² (initial value in figure 4(b)) and from 0.1287 Am² to 0.1033 Am² respectively for 0mm and 2mm.

The results show first that the *z* component of the magnetic moment of 0mm structure (open black circles) decays to 0.075 Am² after one complete cycle of transverse magnetic field. The *y* component of the magnetic moment of 0mm structure (initially null) opposes to the transverse magnetic field and describes a hysteretic curve during the cycle with a final value of -3.6 mAm².

For the 2mm sample (open red triangles) – i. e. the hybrid SC/FM structure with 2 mm thick FM layer) – the *z* component of magnetic moment m_z is larger than for the SC pellet alone by 38 % before the application of the transverse field. After one complete cycle of transverse magnetic field, its value decays to 0.085 Am².

Despite the fact that the 3D model does not give accurate quantitative results, it is clear that the presence of the FM layer increases m_z even after one complete cycle of transverse magnetic field.

When looking more closely on the SC and the FM contribution to both *y* and *z* components of the magnetic moment, we see that the SC contributions of 0mm and 2mm samples are very close. Both SC and FM contributions to the *z* component of the magnetic moment are positive. Then, their addition in the hybrid SC/FM structure leads to the increase of m_z. By contrast, the SC and the FM contributions to the *y* component of the magnetic moment have opposite signs. Indeed the magnetic moment of the superconductor opposes the applied transverse magnetic field while that of the ferromagnet aligns with the applied magnetic field. As a result, the transverse component of the magnetic moment m_y is smaller for the hybrid SC/FM structure (i.e. 2mm) than for the SC pellet alone (0mm).

In what follows, the simulations will be carried in 2D in order to reduce the dispersion of the results. Even though these simulations will not exactly represent the geometry of the hybrid SC + FM, they will already capture the main physics of crossed field effects. Their limitations will be further discussed at the end of this paper, through a comparison between 2D and 3D simulations.

Therefore, most of the following modelling results will be obtained in 2D. Even if it does not represent exactly the geometry of the hybrid SC/FM structure, valuable results can be obtained to improve our understanding of the crossed field effect. A discussion between the results relative to 2D and 3D modelling and their differences is carried out at the end of this paper.

IV. 4. Comparison between 2D modelling of the magnetic moment and experimental results

A large number of cycles of small amplitude transverse magnetic field (12.5 mT) was applied at 50 mT/s by sets of 10 cycles in order to measure the dipolar magnetic moment of several hybrid SC/FM structures. The results are presented in figure 5. The measured samples are those with FM thicknesses of 0, 0.35, 2 and 3 mm and the FM/SC/FM hybrid structure with two FM layers of 1 mm. After 200 cycles we observe that the decay for the sample without FM layer (0mm) reaches 6 % (normalized magnetic moment = 0.94) while the decay decreases monotonically from approximately 5 % to 4.5 % for samples with FM layers of 0.35 mm to 3 mm. The magnetic moment of the FM/SC/FM hybrid structure with 1 mm thick FM layers decays only by 4 %.

For comparison, we model in 2D the SC/FM and the FM/SC/FM structures listed in table 1 (with exclusion of the coax-*x*mm structures) with the same amplitude and sweep rate as in the experiments (i. e. 50 mT/s). Due to the large calculation time, we limit the modelling to 10 cycles. In order to investigate the influence of the sweep rate, all structures are modelled at a sweep rate of 1 mT/s and for the 0mm structure we add the cases of dB_{app}/dt = 5 mT/s and 10 mT/s.

At a given dB_{app}/dt we observe the same order of curves as in experiments, i. e. a monotonic reduction of the decay with the FM thickness and a larger effect in the case of the symmetric FM/SC/FM structure. For dB_{app}/dt = 50 mT/s the modelling results give a slightly larger decay after 10 cycles than the experimental data but the agreement is fair considering the very small decay of less than 1 %. The decay of the magnetic moment after 10 cycles of transverse magnetic field is larger for smaller sweep rates mainly because of a smaller current density in the superconductor and a larger penetration of the shielding currents.

The observed difference between experimental and modelling results at the same sweep rate – i. e. dB_{app}/dt = 50 mT/s – can arise from several causes including (i) J_c difference and inhomogeneity in the measured SC pellet, (ii) limitations of the 2D geometry, (iii) insufficient mesh refinement and convergence criterion, etc.

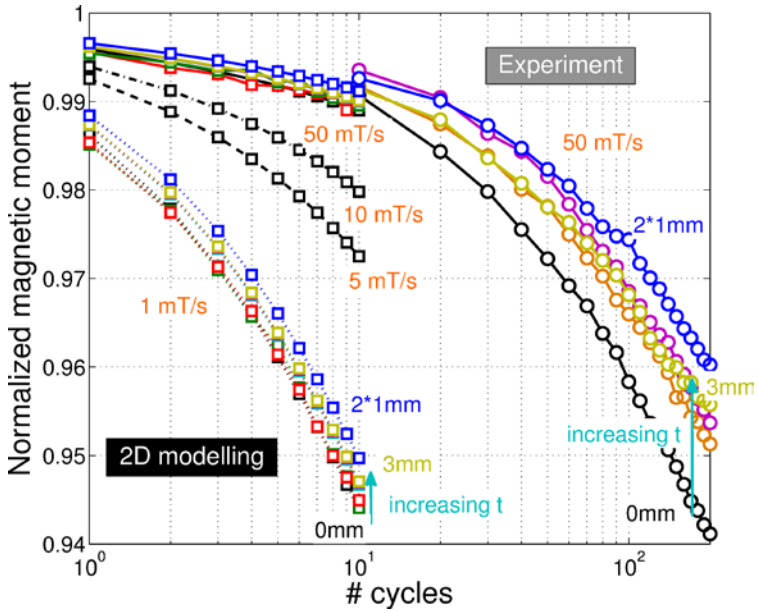

Figure 5: Normalized magnetic moment of samples subjected to several cycles of 12.5 mT transverse magnetic field (along y axis). The experimental results (circles) are obtained with a sweep rate of 50 mT/s (solid lines) on samples with FM thicknesses of 0 mm (black), 0.35 mm (orange), 2 mm (purple) and 3 mm (dark yellow) and on the FM/SC/FM hybrid structure with two FM layers of 1 mm (blue). The 2D modelling results (squares) are obtained with a sweep rate of 1 mT/s (dot lines) and 50 mT/s (solid lines) on samples with FM thicknesses of 0 mm (black), 0.25 mm (green), 0.5 mm (red), 1 mm (light blue), 2 mm (purple) and 3 mm (dark yellow) and on the FM/SC/FM hybrid structure with two FM layers of 1 mm (blue). Additional results on the 0mm structure (black squares) are obtained by 2D modelling with sweep rates of 5 mT/s (dashed line) and 10 mT/s (dashed-dot line).

Another set of modelling results in 2D is obtained for a premagnetized SC/FM structures subjected to one cycle of transverse magnetic field of 100 mT applied with dB_{app}/dt = 1 mT/s, after a flux creep relaxation of 1888 s. We aim at comparing the 2D modelling results to the experimental results obtained (i) by the magnetometer and (ii) by the Hall probe measurements below the surface opposite to the FM disk. The individual contributions of the SC pellet and the FM layer to the total magnetic moment are shown in figure 6 and the total magnetic moment of each structure is plotted in figure 7 as well as their normalized values.

First, we observe that after the flux creep period (and before application of any transverse field) the SC contributions to the magnetic moment of the different structures have decayed from 12.2 Am (see table 1) to approximately 10.1 Am with a spread of 1 % among structures. The smallest magnetic moment is that of the 0mm sample and it increases with the thickness of the FM layer. The 2*1mm structure has the largest magnetic moment. Concerning the initial value of the FM contribution, we can observe on figure 6(b) that it increases proportionally with the thickness of the FM layer. However, as it was shown already, after the magnetization process in 2D and in 3D, even if the total thicknesses of 2mm and 2*1mm are the same, the FM magnetic moment is 13.5 % larger in the latter case. Indeed in the 2mm structure the upper half part of the FM layer is shielded by the lower part resulting in a reduction of the total magnetization while in the 2*1mm structure both 1 mm FM layers see the large magnetic induction in the vicinity of the SC pellet top and bottom surfaces which therefore provides a larger total magnetization.

After one bipolar cycle of 100 mT, the SC magnetic moment decay appears smaller when increasing the FM thickness with a trend to saturate above 1 mm as can be seen in figure 7. For the 2*1mm structure the decay is reduced in a more effective way in comparison to the unilateral SC/FM

structures. It is informative to examine both SC and FM contributions of the magnetic moment. Concerning the FM magnetic moment, all structures present a decay to approximately 80 % of the initial value (cf. figure 7). The total magnetic moment of SC/FM structures (calculated by $m_{SC}^{2D} + ¾\ m_{FM}^{2D}$ as discussed above) is presented in absolute values as inset in figure 7. Two effects can be observed: (i) the increase of the magnetic moment value due to the FM contribution and (ii) the reduced decay of the magnetic moment decay due to the FM layer. In particular, the enhanced action of the symmetrical FM/SC/FM structure can also be observed, similar to what was observed at a smaller amplitude of the transverse field in figure 5.

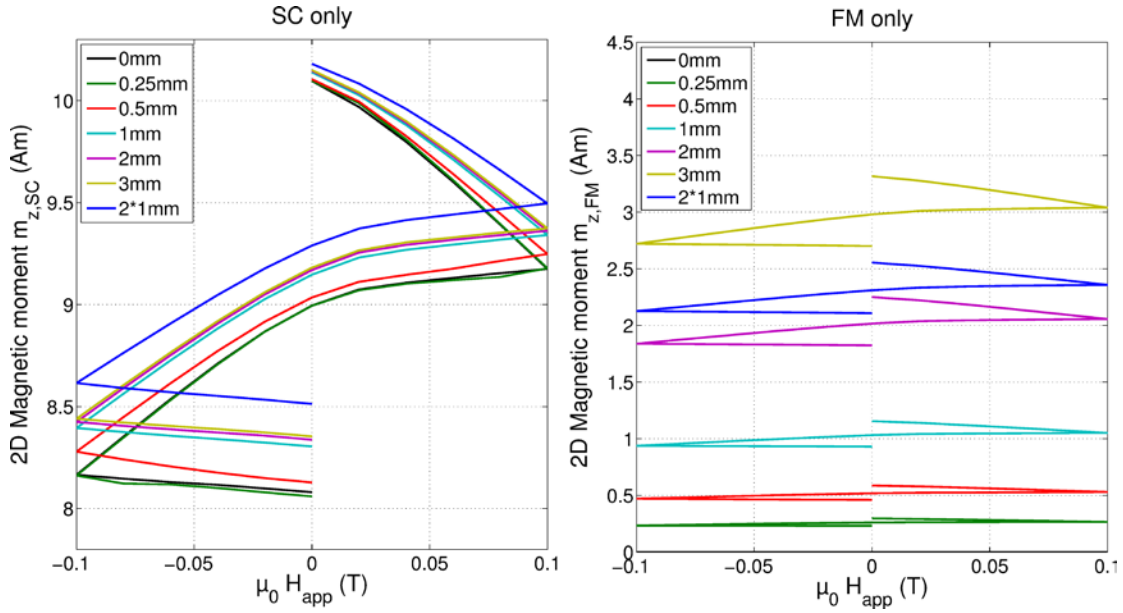

Figure 6: 2D modelling of the separated contributions of the SC pellet (a) and the FM layer (b) to the total magnetic moment of SC/FM structures subjected to one cycle of transverse magnetic field of 100 mT applied with dB_{app}/dt = 1 mT/s. There is obviously no FM contribution for the 0mm sample.

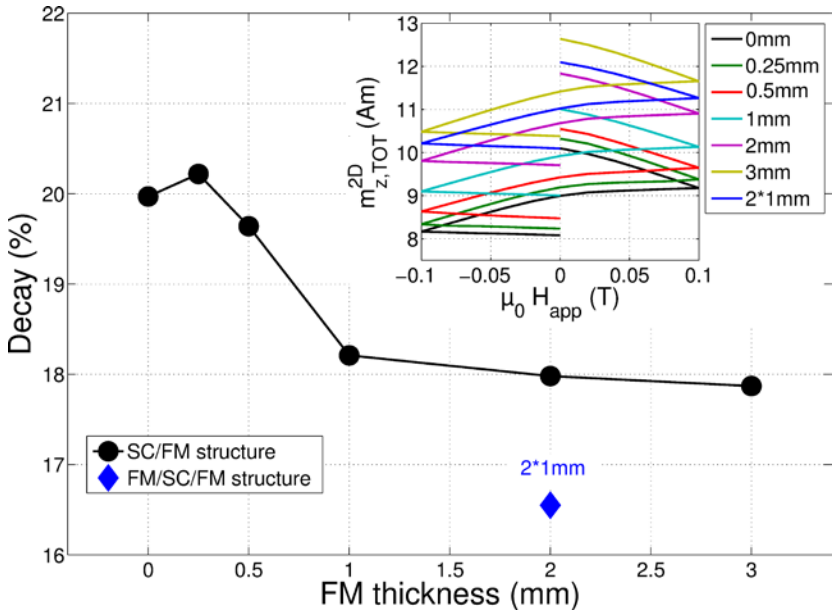

Figure 7: Normalized decay after one complete 100 mT magnetic field cycle obtained by 2D modelling. Inset: absolute values of magnetic moment (in Am) of whole SC/FM structures subjected to one cycle of transverse magnetic field of 100 mT applied with dB_{app}/dt = 1 mT/s modelled in 2D.

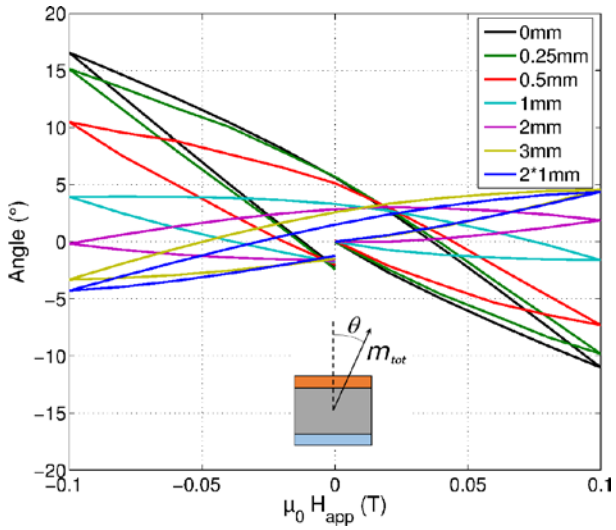

Figure 8: Tilt angle of the total magnetic moment with respect to the axis (inset) for SC/FM structures subjected to one cycle of transverse magnetic field of 100 mT applied with dB_{app}/dt = 1 mT/s.

The transverse magnetic field does not affect only the axial component of the magnetic moment. As shown by 3D modelling in figure 4(a), the transverse components of the magnetic moment of both SC and FM parts of the SC/FM structure evolve also during the cycle of transverse applied magnetic field. Therefore, the total magnetic moment of the structure depends on the relative amplitudes of its transverse and axial components and its angle with respect to the axis of the structure changes with the applied magnetic field. We characterize this situation by analysing the tilt angle of the total magnetic moment for one cycle of a transverse field for several thicknesses of the FM layer (see figure 8).

For the 0mm structure, it can be observed that the magnetic moment tilts in the direction opposite to the magnetic field because of the induced superconducting currents near top and bottom. In the negative part of the cycle, at $\mu_0 H_{app}$ = - 0.1 T, the tilt angle is even larger (16.6°) that at $\mu_0 H_{app}$ = 0.1 T (11°) showing a larger penetration of the transverse superconducting currents to the detriment of the currents providing the axial magnetization. On increasing the FM thickness, this tilt angle is reduced and even reversed for FM thicknesses above 2 mm. In this regime the transverse magnetic moment of the SC/FM structure then varies in phase with the applied transverse magnetic field. The 2*1mm structure presents similar variations for increasing magnetic fields up to $\mu_0 H_{app}$ = 0.1 T, and a larger negative value of the tilt angle at $\mu_0 H_{app}$ = - 0.1 T.

These results shows that, under a transverse magnetic field, the FM layer tends to increase its magnetic moment in phase with the applied magnetic field, whereas the SC tends to expel flux from its bulk and develop a counter magnetization. The resulting magnetic moment of the structure is thus a compromise between ferromagnetic and diamagnetic individual responses which depends on the thickness of the FM layer.

IV. 5. 2D modelling of the local magnetic induction

The local magnetic induction is also calculated along the axis of the SC/FM structures and in particular at the location of the Hall probe in the experiments z = - 4.5 mm (i.e. 2 mm below the SC surface for SC/FM structures and 1 mm below the bottom 1 mm FM layer surface for the 2*1mm structure, as shown schematically on the inset of figure 9(a)). The modelling results are presented in figure 9. The magnetic induction increases nonlinearly with the FM thickness, starting from 171.5 mT for the structure without FM layer to 176.8, 181.7, 185.9, 189.2, 191.8 mT for FM thicknesses of 0.25, 0.5, 1, 2 and

3 mm (cf. figure 9(a)). These numbers correspond to increments by 3, 5.9, 8.4, 10.3, and 11.8 % respectively. In the case of the 2*1mm structure, the magnetic induction drops to 89.2 mT of the magnetic induction calculated for 0mm structure at the same elevation z and to 82.15 mT at a constant distance of 2 mm from (corresponding respectively to 52 % and 47.9 % of the magnetic induction calculated for the SC pellet alone). The decay of the normalized magnetic induction after one 100 mT magnetic field cycle as a function of the FM thickness is displayed as inset. Here again, the FM layer seems beneficial since it helps in obtaining larger magnetic flux densities. Two effects can be observed. First, there is a smaller decay which tends to reach saturation for the structures with the thicker FM layers and secondly, a better relative protection against transverse field is provided by the symmetrical FM/SC/FM structure. Specifically, the magnetic induction decay after one cycle of 100 mT calculated in 2D modelling can be compared to measured values for the 0mm and the 1mm structures shown in figure 4. Experimentally the magnetic induction decays to 71.7 % and 81.5 % from their initial value respectively for 0mm and 1mm structures, while the 2D calculations give respective values of 77.9 % and 80 %. Even if the magnetic induction decay for the 0mm structure seems underestimated in the 2D modelling results, there is a fair agreement of the orders of magnitude.

V. Discussion

In order to explain how the FM layers influence the magnetic moment and the magnetic induction around the SC/FM structures, we investigate (i) how the supercurrents in the SC pellet are affected in the presence of the FM layer and (ii) how the magnetization of the FM layer varies considering the nonlinear magnetic behaviour of this material and, in particular, its saturation magnetization value.

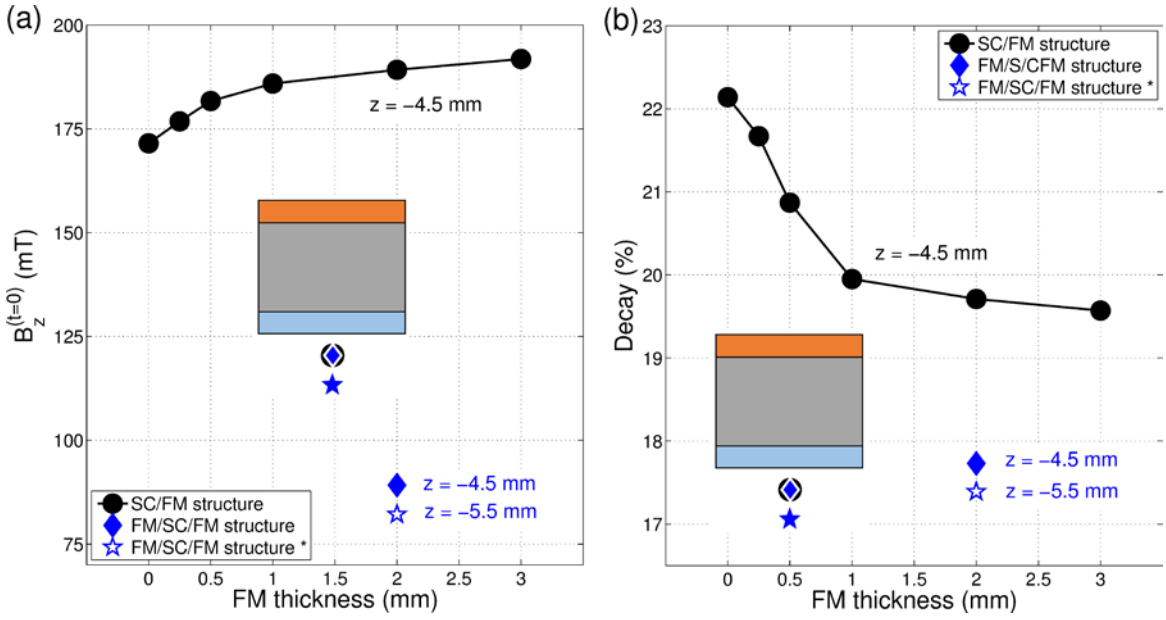

Figure 9: Modelled initial value of the magnetic induction B_z as a function of the FM thickness at z = - 4.5 mm (i.e. 2 mm below the SC surface for SC/FM structures and 1 mm below the bottom 1 mm FM layer surface for the 2*1mm structure) by 2D modelling on SC/FM structures subjected to one cycle of transverse magnetic field of 100 mT applied with dB_{app}/dt = 1 mT/s. The value calculated 2 mm below the 2*1mm structure (i.e. at z = -5.5 mm) is added and labelled with a star in order to be compared to the value at the same physical distance below the entire structure. Inset: Schematic z elevations of the calculations. (b) Decay of the magnetic induction after one 100 mT magnetic field cycle as a function of the FM thickness. The decay is normalized with respect to the corresponding values before applying the transverse magnetic field cycle.

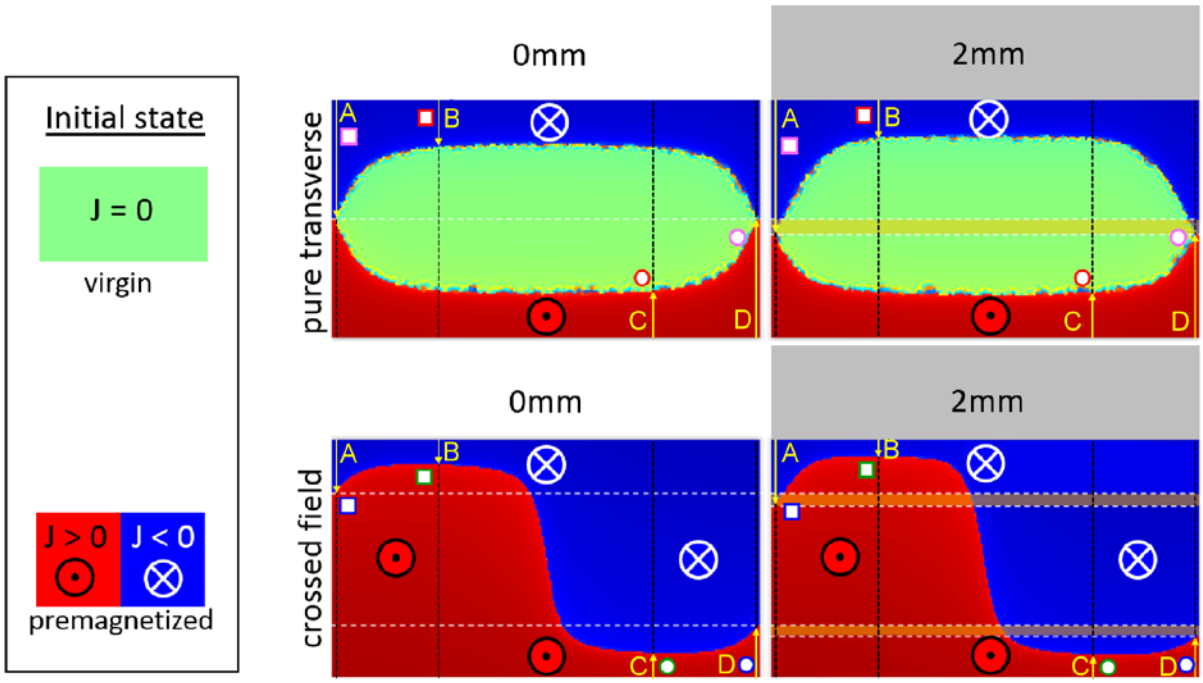

Figure 10: Distribution of the superconducting currents in the SC pellet in the case of (top) the "virgin" state and (bottom) the "premagnetized" state (see inset and text). The left part illustrates the case of the 0mm structure (SC pellet alone) and the right part illustrates the case of the 2mm structure where the 2 mm FM layer is located above the SC pellet. All distributions correspond to a transverse magnetic field increased up to $\mu_0 H_{app}$ = 0.1 T. For clarity, the critical current density equals 1.25 10^8 A/m² i. e. half the J_c value used in the main part of the paper (see text). Coloured circles and squares correspond to the labels of the results plotted in figure 11.

V. 1. Penetration depth d_{pen}

First, we study the penetration of the superconducting currents, induced by the transverse magnetic field, from both surfaces, the top surface which is in contact with the FM layer and the bottom surface which is opposite to the FM layer. We study the current distribution when a transverse magnetic field is applied by 2D modelling in two situations: (i) a SC pellet without premagnetization, i.e. in the virgin state ("pure transverse" case) and (ii) a SC pellet which was premagnetized in the *z* direction ("crossed field"). Figure 10 shows the current distribution in both cases for the 0mm structure (SC pellet alone), left part of the figure and the 2mm structure (right part of the figure). The 2 mm FM layer is located above the SC pellet. All distributions correspond to a transverse magnetic field increased up to $\mu_0 H_{app}$ = 0.1 T. For clarity, the critical current density was chosen as 1.25 10^8 A/m² i. e. half the J_c value used in the main part of the paper, in such a way that the penetration is larger and the differences between the two cases are amplified.

We calculate and we report in figure 11 the penetration depth d_{pen} at four radii (vertical black dashed lines of figure 10), in order to observe the relative penetration inside (locations B and C) and at the vicinity of the lateral surface (locations A and D) of the SC pellet. The penetration depths are counted from the top surface (close to the FM layer) for the negative *y* (depicted by squares in figures 10 and 11) and from the bottom surface (opposite to the FM layer) for the positive *y* (depicted by circles in figures 10 and 11). Additional results concerning the symmetrical 2*1mm structure are plotted with upward and downward triangles (cf. figure 11).

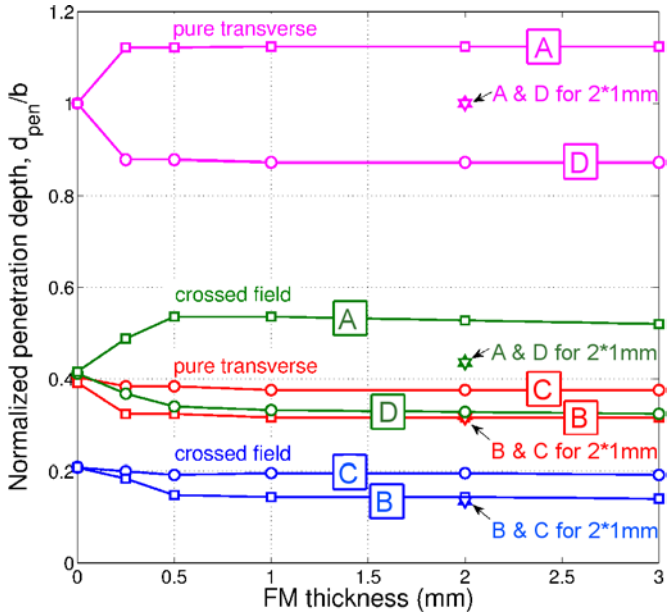

Figure 11: Penetration depths (normalized to the half-height of the SC pellet *b*) of the superconducting currents as a function of the FM thickness in the case of the "virgin" state subjected to a transverse field and the "premagnetized" state subjected to a crossed field (see text). Squares correspond to the penetration from the surface close to the FM layer and circles correspond to the penetration from the surface opposite the FM layer. Additional results concerning the symmetrical 2*1mm structure are plotted with upward and downward triangles. All distributions correspond to a transverse magnetic field increased up to $\mu_0 H_{app}$ = 0.1 T. The critical current density equals 1.25 10^8 Am^{-2}.

We first consider the case of the 0mm structure, i. e. in the absence of FM layer. As can be seen in the left part of figure 10, the structure is symmetric and the penetration depths from either top (square) or bottom (circle) surfaces are equal. In the case of the pure transverse field, the penetration is complete near the lateral surfaces but the penetration is partial at locations B and C. When the sample is premagnetized (bottom left part of figure 10), the initial currents distribution is such that the currents are positive (red) in the whole left half of the pellet and negative (blue) in the right half. Under a 0.1 T crossed field, we observe a step shape of the current distribution. Despite of the strong current distribution modification induced by the transverse or crossed field, the positive and negative currents still counterbalance each other's and it is verified that the integral of the current density over the total SC surface is null.

When a FM layer is placed on the top of the SC pellet, an asymmetry arises between the top and the bottom parts of the SC pellet. The case of a 2 mm FM layer structure is shown in the right part of figure 10. In the case of the pure transverse field, the penetration is complete but, in opposition to the previous case without FM layer, at the sides, the penetration of the negative currents from the top surface (close to the FM layer) is deeper than the positive currents from the bottom surface. As the total current has to be null, the penetration inside the SC pellet is modified accordingly. We calculate that at locations b and c the penetration of the negative currents from the top surface is smaller than for the 0mm structure while the penetration of the positive currents from the bottom surface is close to the value for the SC pellet without FM layer. Again, the total current is verified to equal zero.

In figure 11, the penetration depths at the four locations discussed above are plotted as a function of the FM thickness. We can see the asymmetry of the penetration depths due to the presence of the FM layer appears for the smallest modelled thickness (d_{FM} = 0.25 mm). Above a given thickness of the FM layer of 0.25 mm, hereafter called $d^{//}$, the difference in penetration depths is almost independent of the FM thickness. In the case of the 2*1mm structure a symmetry is recovered. The penetration near the

lateral surfaces (magenta triangles) is the same as without FM layers so $d_{pen}/b = 1$. The penetration at $\pm a/2$ (red triangles) is the same as the penetration of the negative currents below the 1mm FM thick 1mm asymmetrical structure (red squares) i.e. $d_{pen}/b = 0.32$.

In the crossed magnetic field configuration, we observe an increase of d_{pen}/b for the negative currents in comparison to the value for the 0mm structure (it now equals 0.53, green squares), and a decrease for the normalized penetration depth of the positive currents ($d_{pen}/b = 0.37$, green circles). In the case of the symmetrical 2*1mm structure, the penetration near both lateral surfaces (green triangles) is slightly higher than without FM layers. Here again, because of the fact that the total current equals zero, the penetration depth inside the SC pellet below the FM layer (blue squares) is reduced while it remains almost unaffected by the FM layer in the opposite side (blue circles). Let us remark that here the influence of the FM layer increases for thicknesses increasing up to a threshold thickness of 0.5 mm, hereafter called d^+ (while the threshold thickness in the pure transverse case $d^{//}$ was 0.25 mm), before to level off and to become almost independent of the FM thickness. Additional results (not shown here) on 2D modelling with $J_c = 2.5\ 10^8$ A/m² (twice that of this section) show that the threshold FM thickness rises to 1 mm for crossed field cases.

The same kind of threshold FM thickness has already been observed in a previous study concerning the contribution of ferromagnetic sections placed in contact to bulk high temperature superconductors (similar to our asymmetrical SC/FM structures) in order to enhance their trapped field [10]. In this previous study, the increase of the local magnetic induction measured at the centre of the surface opposite to the FM layer plotted as a function of the FM thickness was shown to exhibit a 'kink'. According to the 2D modelling, this kink corresponds to the full saturation of the ferromagnet and a threshold thickness d^* below which saturation occurs is roughly estimated by using a simple analytical model based on magnetic flux conservation. With the rough estimation of $d^* \approx (J_{c0}\ a^2) / (6\ M_{sat})$, where $J_c = 2.5\ 10^8$ A/m², $a = 4.5$ mm and $\mu_0\ M_{sat} = 1.4$ T, we find $d^*(J_c) = 0.76$ mm and $d^*(J_c/2) = 0.38$ mm which is a value close to the threshold FM thicknesses $d^{//}$ and d^+ for samples subjected to pure transverse or crossed magnetic fields which are obtained from the penetration depths values shown in figure 11.

From these results, we conclude that, because the FM layer is subjected to a concentration of magnetic flux, a higher magnetic induction develops at the corner of the SC pellet below the FM layer. This enhances the penetration of the currents in this region, while the penetration on the opposite side is nearly unaffected by the FM layer. Because of the net current has to be zero, the penetration inside the pellet directly below the FM layer is therefore reduced.

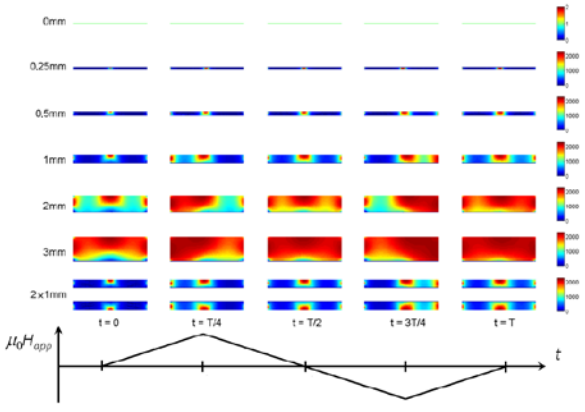

Figure 12: Distribution of the relative permeability μ_r of the FM layer of the SC/FM structures after their magnetization and the application of the transverse magnetic field. The column $t = 0$ corresponds to the end of the flux creep period (1888 s) following the magnetization process. The subsequent columns correspond to each quarter of period of one cycle of 100 mT transverse magnetic field (as sketched in the bottom part). The modelling results are obtained with $J_c = 2.5\ 10^8$ Am^{-2}.

V. 2. Saturation of the FM layer and threshold thickness d^+

Now, in order to examine in details the cause of the kink at a threshold thickness d^+ in the plot of the penetration depth of the superconducting currents inside the SC pellet with respect to the thickness of the FM layer in crossed field configuration, we turn to the behaviour of the FM layer itself. The 2D modelling allows us to calculate the relative permeability μ_r of the FM layer during the magnetization and the application of the transverse magnetic field. In figure 12 we plot the distribution of μ_r for the SC/FM structures at $t = 0$ corresponding to the end of the flux creep period following the magnetization process, as well as for each quarter of period of one cycle of 100 mT transverse magnetic field (as sketched in the bottom part of the figure). The modelling results are obtained with $J_c = 2.5\ 10^8$ A/m².

Below its full saturation, the FM layer subjected to the trapped magnetic flux of the SC pellet ($t = 0$) will drive the majority of the flux lines radially towards its sides and thus will shield the free space above it. This situation is shown in the left column of figure 12 ($t = 0$): Most of the FM layer is subjected to a large magnetic flux which leads to its saturation and the drastic drop of the relative permeability when the FM thickness is below 1 mm (including the 2*1mm structure). There still exists a zone along the axis where the magnetic field is low enough to keep the ferromagnet below its saturation and therefore a high value (above 2000) of the relative permeability. For thicknesses larger than 2 mm, only the bottom part of the FM layer is saturated and a symmetric distribution of μ_r can be observed (light blue area for the 2mm structure and red area for the 3mm structure).

We now examine how the magnetic permeability of the FM layer is modified when a transverse magnetic field is applied. As the transverse magnetic field increases up to 100 mT ($t = T/4$), the magnetic flux is decreased in the left hand part of the layer and μ_r increases accordingly. The right hand part of the FM layer remains saturated as it was already the case before. At $t = T/2$, a symmetrical situation is recovered but the trapped field of the SC pellet has been slightly reduced in the process and therefore, the relative permeability has increased as can be seen when comparing $t = 0$ and $t = T/2$ for the 2mm structure. When the field is reversed, the magnetic flux is increased in the left part of the layer and μ_r decreases in that region. Let us remark that (i) the 2*1mm structure behaves almost perfectly like two independent FM layers of a 1mm structure and (ii) for FM thicknesses of 0.25 and 0.5 mm, the μ_r distribution is not strongly affected by the transverse magnetic field, at the exception of a slight expansion of the high magnetic permeability region along the axis. This is because the FM layer is always subjected to a magnetic flux large enough to lead to the full saturation in the whole FM layer. These results are in good agreement with the threshold thickness determined in section V. 1.

The results shown in figures 10-11, the apparent limited influence of the FM layer on the magnetic moment (figure 6(a) and figure 7(b)), and the magnetic induction below the bottom surface figure 9(b)) when the FM thickness exceeds 1 mm tend to show that the highest beneficial effect of the FM layer in such asymmetrical SC/FM structures is obtained for a FM thickness equalling d^+.

V. 3. Alternative symmetrical FM/SC/FM structure

It has been shown experimentally (figure 5) and numerically (figure 7(b) and figure 9(b)) that, among all the premagnetized structures subjected to crossed field, the 2*1mm structure presents the smallest decay of the normalized values of both magnetic moment and magnetic induction, as a FM layer of optimal thickness (close to d^+) protects the SC pellet from the transverse field. However the FM layers shield the trapped induction above and below the SC pellet making them of little use for most applications (rotating machines, levitation …). Therefore, we study a symmetrical SC/FM structure, here after called coax-*x*mm, where the FM layers (thickness of *x* mm) are placed on the sides rather than on the top and bottom surfaces of the SC pellet. In practice this structure is a FM ring surrounding the SC pellet (cf. figure 1 (d)). Axisymmetric 2D modelling however cannot be carried out because of the

symmetry breaking due to the crossed fields. This structure was then modelled in 2D by its *y*-*z* cross section and infinite along the *x* direction as shown schematically in figure 1 (h).

Figure 13 presents the distribution of B_z at the end of the flux creep period for several SC/FM structures, i.e. 0mm, 1mm, 2*1mm and coax-1mm. Their respective magnetic moment after magnetization are reported in table 1. As can be seen in figure 13, above the top FM layer for 1mm and 2*1mm and also below the bottom FM layer in the latter structure, the magnetic field is shielded. In the case of the coax-1mm structure, the return magnetic flux lines are concentrated inside the FM layers (around 1 T in figure 13 (d)). For this structure, the magnetic field is shielded on the sides of the structure. When comparing to the 0mm structure, the magnetic field is preserved above and below the SC pellet.

Figure 14 presents the distribution of μ_r at the end of the flux creep period for coax-xmm structures of several thicknesses of the FM layers (x = 0.25, 1, 2 and 3 mm). For a thickness below 1 mm, the large magnetic flux density in FM layers leads to their saturation as can be seen in figure 14 (a and b). For thicker FM layers of 2 and 3 mm, the magnetic flux density inside the FM layers is not large enough to saturate the material and the magnetic permeability remains large (μ_r > 1000) in most of the ferromagnet. In this 2D geometry, the threshold thickness $d^{\#}$ seems to be slightly higher than 1 mm. Therefore, like for the *x*mm and the 2**x*mm structures, a FM thickness of x = 1 mm seems to be also a reasonable optimum for the coax-*x*mm structure.

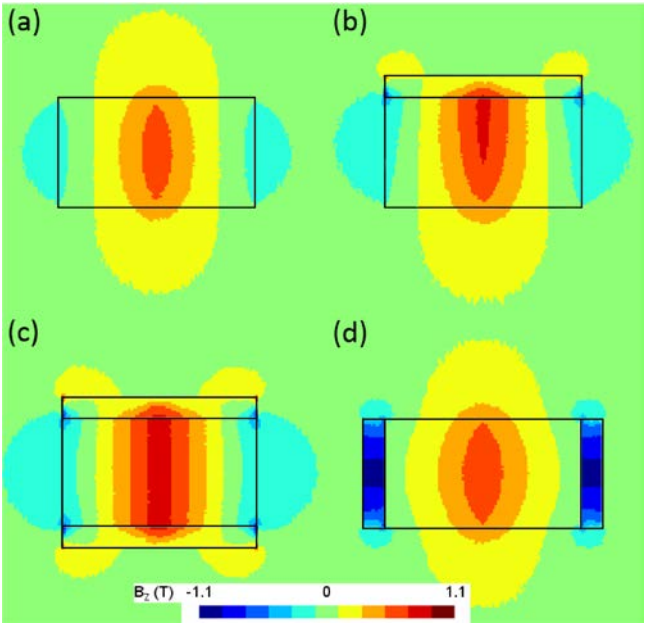

Figure 13: Distribution of the B_z at the end of the flux creep period (1888 s) for (a) 0mm, (b) 1mm, (c) 2*1mm and (d) coax-1mm.

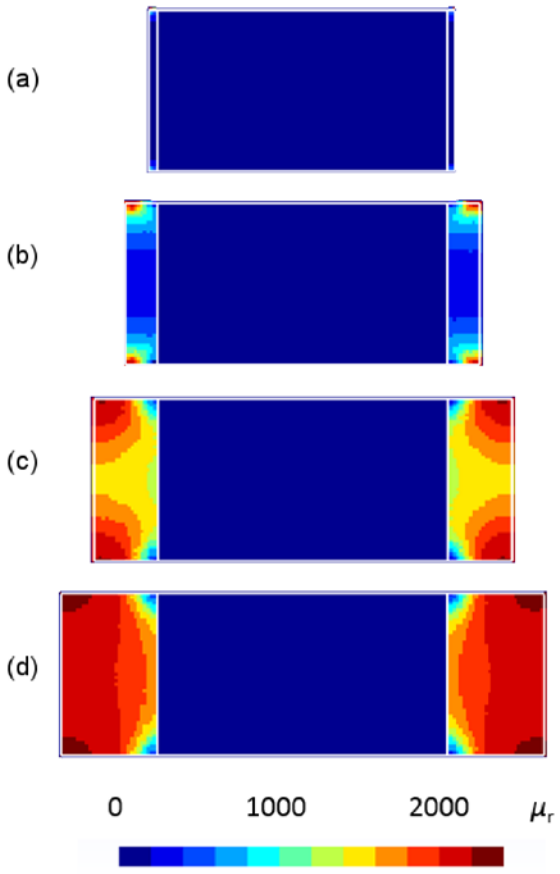

Figure 14: Distribution of the relative permeability μ_r of the FM layers at the end of the flux creep period (1888 s) for (a) coax-0.25mm, (b) coax-1mm, (c) coax-2mm and (d) coax-3mm.

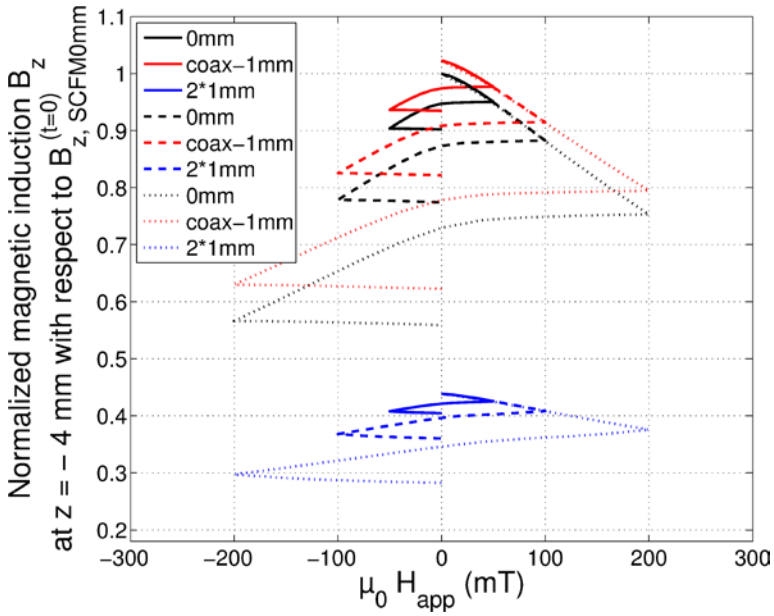

Figure 15: Magnetic induction calculated at z = - 4 mm by 2D modelling on 0mm, coax-1mm and 2*1mm structures subjected to one cycle of transverse magnetic field of 50, 100 and 200 mT applied with dB_{app}/dt = 1 mT/s.

The local value of the magnetic induction at z = - 4 mm for the premagnetized structures presented in figure 14 (a), (c) and (d) and subjected to one cycle of transverse magnetic field of 50, 100 and 200 mT are plotted in figure 15 as a function of the applied magnetic field. The data is normalized with respect to the initial magnetization of the 0mm structure. Similarly to the results presented in figure 9 for $\mu_0 H_{app}$ = 100 mT at z = - 4.5 and 5.5 mm, the 2*1mm structure exhibits a shielding due to the bottom 1 mm FM layer. The magnetic induction is reduced to 44 % of that of the 0mm structure while its magnetic moment is increased by 18.6 % as shown in table 2. By contrast, the initial value of the magnetic induction for the coax-1mm structure is increased by 2.3 % while its magnetic moment is reduced to 56.5 % of that of the 0mm structure as shown in table 2.

The decays after one cycle of magnetic field of 50, 100 and 200 mT are respectively given as 0.90, 0.78 and 0.56 for 0mm, 0.92, 0.82 and 0.64 for 2*1mm and 0.91, 0.80 and 0.61 for coax-1mm. The 2*1mm structure is the most immune structure against the crossed field but the drawback is that the magnetic induction level is strongly reduced. By contrast, the coax-1mm structure presents also a better protection than the 0mm structure, with the additional advantages to slightly boost the local magnetic induction value and to shield the sides of the structure.

V. 4. Critical comparison of 2D and 3D modelling

The advantage of 2D modelling are (i) the absence of longitudinal currents, (ii) faster calculations for a given number of elements, and (iii) larger numbers of elements for a given calculation. However, as mentioned several times above, great care has to be taken in interpreting results from a 2D analysis. In order to illustrate this point, we discuss in more details the case of a coax-3mm structure premagnetized along the z direction and subjected to a transverse magnetic field $\mu_0 H_{app}$ = 0.1 T along the y axis (cf. figure 14). We plot in figure 16 (a) the distribution of the current density in the SC pellet (arrows) and the relative permeability μ_r of the FM layer (filled iso-values) modelled in 2D. We observe the step shape in the superconducting current distribution. This is characteristic of the penetration of superconducting current layer shielding the transverse magnetic field that superimposes to the initial current distribution sustaining the premagnetization. The μ_r distribution is that of figure 14 (d). Because of the applied transverse field, the area of the saturated FM layer (μ_r = 1) increases slightly in the upper right and lower left corners of the FM layer while it is reduced in the opposite corners. The amplitude of the magnetic field is not sufficient to induce saturation on a larger area on these 3 mm thick FM layers.

For comparison, we modelled in 3D a 3 mm thick FM ring around a SC pellet of same diameter and height than the width and height of the 2D structure. The spatial resolution in 3D is lower than in 2D as the characteristic length of the tetrahedrons in 3D is 300-500 µm while the characteristic length of the triangles in 2D is only 70 µm. In order to save time, we also use a less severe convergence criterion (a residue of 10^{-3} instead of 10^{-6} to 10^{-10} for 2D modelling). A lower precision, therefore, is reached in the 3D results.

The distribution of the critical current density in the SC pellet (arrows) and the relative permeability μ_r of the FM layer (filled iso-values) are shown in figure 16 (b) for a quarter of the geometry in the x = 0 plane (the same plane as for the FM/SC/FM bar in 2D) and in the y = 0 plane (the plane orthogonal to the transverse magnetic field direction). The μ_r distribution is also plotted in the additional plane z = 0 for the FM layer. There is a fair agreement between 2D and 3D modelling results in the x = 0 plane for both J_c and μ_r distributions. In the 3D model, the step shape characteristic of the J_c distribution can also be observed, although with a slightly lower maximum value of the current density. Similarly, the μ_r distribution is similar to the 2D results, with however a lower saturation of the FM layer in the internal corner similar to the 2D results. The 2D and 3D results are markedly different in the y = 0 plane. Because of the demagnetizing field of the SC pellet, the magnetic flux lines applied in the y

direction are concentrated on the sides of the SC pellet ($x = \pm a$, $y = 0$) while they are diluted along the y-axis. As a result, the relative permeability of the FM layer is reduced in the $y = 0$ plane in comparison to the μ_r distribution in the $x = 0$ plane and an eye-shape distribution can be observed in the $z = 0$ plane in figure 16 (b) for a quarter of the geometry, and the full cross section of this distribution is presented in the inset (c) of figure 16. In the $y = 0$ plane, the current flows along the y direction in the inner part of the SC pellet but it follows the borders of the pellet and is in-plane in order to shield the applied magnetic field. This distribution is fundamentally different from that in the $x = 0$ plane. The complex current flow thus contribute differently to the total magnetization than what a simpler 2D model would predict.

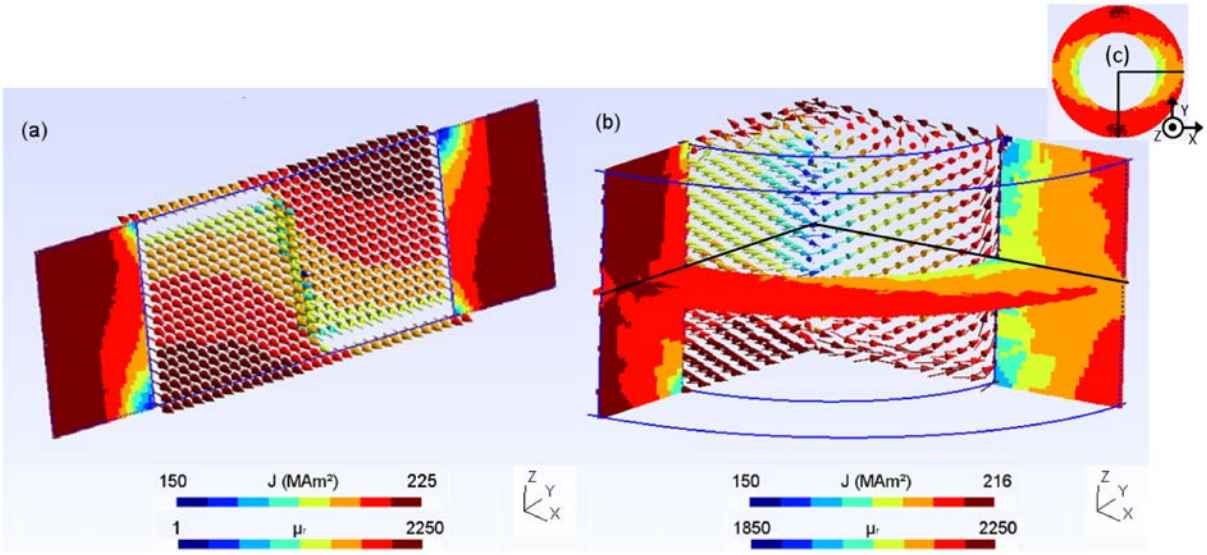

Figure 16: Distribution of the current density in the SC pellet (arrows) and the relative permeability μ_r of the FM layer (filled iso-values) for a premagnetized coax-3mm structure modelled (a) in 2D and (b) in 3D. The results are shown at a transverse magnetic field $\mu_0 H_{app} = 0.1$ T in the plane $x = 0$ for the 2D model and in a quarter of the geometry in the planes $x = 0$ and $y = 0$ as well as the additional plane $z = 0$ for the FM layer in the 3D model also displayed in the inset (c).

VI. Conclusions

In this paper we investigated, both experimentally and numerically, the effect of a FM disk of various thicknesses placed in contact with a SC pellet in a crossed field configuration. The local magnetic induction and the magnetic moment of the SC/FM structure were characterized experimentally with bespoke systems.

2D and 3D modelling were carried out to (i) calculate the individual SC and FM contributions to the magnetic moment, as well as the magnetic induction at the vicinity of the studied structures, (ii) study the penetration of the shielding currents against this transverse field and (iii) examine the influence of the FM layer and its possible saturation on the SC pellet behaviour for various configurations and FM thicknesses.

The 3D model results are in good qualitative and quantitative agreement with the experimental results but the low spatial and numerical resolutions of the 3D model make it sometimes difficult to obtain enough details for small magnetic field amplitudes and thin FM layer.

The magnetic moment was shown to increase linearly with the thickness of the FM layer when it is placed on the top (and/or bottom) plane surface of the SC pellet, while it decreases when the FM

layer is placed on the sides. Both magnetic moment and magnetic induction suffer from a smaller decay under transverse magnetic fields when the structures are covered by a FM layer.

We show that 2D modelling results can be corrected in order to be compared to the experimental and 3D modelling results. The correction is based on the differences of demagnetizing effects in each geometry. With this correction, the 2D model correlates well with the main characteristics observed experimentally for the magnetic moment and the local magnetic induction. This model shows how the currents distribution inside the SC pellet is distorted because of the presence of a FM layer in unilateral SC/FM structures while still keeping a null net current across the cross section of the SC pellet. A threshold thickness is determined, which corresponds to the experimental observation of a saturation of the beneficial effect of the FM layer on the magnetization decay due to the crossed field. Distributions of the relative permeability μ_r for several structures support this evidence by showing that FM layers thinner than this threshold thickness are saturated by the pre-existent magnetization of the SC pellet.

In summary, we find, in the crossed field configuration, that (i) the beneficial effect of the FM layer on the magnetic moment increases monotonically with the FM thickness, (ii) the improvement becomes marginal above a given thickness d^+, and (iii) this threshold thickness is related to the saturation magnetization of the ferromagnetic material. We show also that a symmetrical FM/SC/FM structure with two 1 mm FM layers presents a stronger effect against the crossed magnetic field than all unilateral SC/FM structures.

As an additional study, a comparison of 2D results between a symmetrical FM/SC/FM structures and the SC pellet alone shows that placing the FM layers on the top and bottom surfaces of the SC pellet reduces crossed field effects with the drawback of shielding strongly the magnetic induction. Placing the FM layers on the sides of the SC pellet also reduces crossed fields effects, but with the additional advantage of increasing slightly the local magnetic induction value above and below the structure while shield its sides.

Finally we show the distributions of the current density in the SC pellet and the relative permeability in the FM layers for a cylindrical SC pellet surrounded by a 3 mm thick FM ring subjected to a crossed field. The 3D model is compared to its 2D approximation consisting of an infinite SC bar with two FM layers on its sides. It is observed that the models agree well for describing the current distributions in the cross section parallel to crossed fields. The 3D model shows however different results in the plane perpendicular to crossed fields. 2D models are thus very helpful in understanding crossed field effects, but fail in describing finer characteristics of the shielding currents.

Acknowledgments

The research was funded through the University of Liège (ULg) and an ARC grant for Concerted Research Actions, financed by the French Community of Belgium (Wallonia-Brussels Federation), under reference ARC 11/16-03. We thank S. Debois and his grandfather for the realization of the insertion tool.

References

[1] Tomita M and Murakami M 2003 *Nature* **421** 517

[2] Teshima H, Morita M and Hirano H 2006 *J. Phys.: Confer. Series* **43** 1031

[3] Durell J H, Dennis A R, Jaroszynski J, Ainslie M D, Palmer K G B, Shi Y-H, Campbell A M, Hull J, Strasik M, Hellstrom E E and Cardwell D A 2014 *Supercond. Sci. Technol.* **27** 082001

[4] Zhou D, Izumi M, Miki M, Felder B, Ida T and Kitano M 2014 *Supercond. Sci. Technol.* **25** 103001

[5] Hull J R and Strasik M 2010 *Supercond. Sci. Technol.* **23** 124005

[6] Zhen Huang, Wei Xian, Min Zhang, Chudy M, Chen Y, Zhaoyang Zhong, Baghdadi M, Wei Wang, Spaven F, Matsuda K and Coombs T A 2013 *IEEE Trans. Appl. Supercond.* **23** 5200204

[7] Werfel F N, Floegel-Delor U, Rothfeld R, Riedel T, Goebel B, Wippich D and Schirrmeister P 2012 *Supercond. Sci. Technol.* **25** 014007

[8] Granados X, Torner M, Puig T and Obradors X 2007 *IEEE Trans. Appl. Supercond.* **17** 1629–1632

[9] Philippe M P, Fagnard J F, Kirsch S, Xu Z, Dennis A R, Shi Y H, Cardwell D A, Vanderheyden B and Vanderbemden P 2014 *Physica C* **502** 20

[10] Philippe M P, Ainslie M, Wéra L, Fagnard J F, Dennis A R, Shi Y-H, Cardwell D A, Vanderheyden B and Vanderbemden P 2015 *Supercond. Sci. Technol.* **28** 095008

[11] Naito T, Mochizuki H, Fujishiro H and Teshima H 2016 *Supercond. Sci. Technol.* **29** 034005

[12] Noudem J, Meslin S, Horvath D, Harnois C, Chateigner D, Ouladdiaf B, Eve S, Gomina M, Chaud X and Murakami M 2007 *J. Am. Ceram. Soc.* **90** 2784-2790

[13] Lousberg G P, Fagnard J F, Chaud X, Ausloos M, Vanderbemden P and Vanderheyden B 2011 *Supercond. Sci. Technol.* **24** 035008

[14] Baskys A, Patel A, Hopkins S, Kenfaui D, Chaud X, Zhang M and Glowacki B.A. 2014 *J. Phys.: Confer. Ser.* **507** 012003

[15] Del-Valle N, Agramunt-Puig S, Navau C and Sanchez A 2012 *J. Appl. Phys.* **111** 013921

[16] Gony B, Berger K, Douine B, Koblischka M. R. and Lévêque J 2015 *IEEE Trans. Appl. Supercond.* **25** 6965615

[17] Zou J, Ainslie M D, Hu D, Cardwell D A 2016 *IEEE Trans. Appl. Supercond.* **26** 8200605

[18] Philippe M P, Fagnard J F, Wéra L, Morita M, Nariki S, Teshima H, Caps H, Vanderheyden B and Vanderbemden P 2016 *J. Phys.: Conf. Ser.* **695** 012003

[19] Gurevich A and Küpfer H 1993 *Phys. Rev. B* **48** 6477

[20] Cardwell D A *et al.* 2005 *Supercond. Sci. Technol.* **18** S173

[21] Qiu M, Huo H K, Xu Z, Xia D, Lin L Z, and Zhang G M (2005) Technical Analysis on the Application of HTS Bulk in “Permanent Magnet” Motor. IEEE Trans. Magn. 15:3172-3175

[22] Clem J R 1982 *Phys. Rev. B* **26** 2463–2473

[23] Fisher L M, Kalinov A V, Savel’ev S E, Voloshin I F, Yampol’skii V A, LeBlanc M A R and Hirscher S 1997 *Physica C* **278** 169

[24] Badía-Majós A and López C 2007 *Phys. Rev. B* **76** 054504

[25] Romero-Salazar C and Perez-Rodriguez F 2004 *Physica C* **404** 317–321

[26] Brandt E H and Mikitik G P 2007 *Phys. Rev B* **76** 064526

[27] Hong Z, Vanderbemden P, Pei R, Jiang Y, Campbell A M and Coombs T A 2008 *IEEE Trans. Appl. Supercond.* **18** 1561-1564

[28] Campbell A M 2011 *Supercond. Sci. Technol.* **24** 091001

[29] Celebi S, Sirois F and Lacroix C 2015 *Supercond. Sci. Technol*. **28** 025012

[30] Pérez-Rodríguez F, LeBlanc M A R and Gandolfini G 2001 *Supercond. Sci. Technol.* **14** 386-397

[31] Vanderbemden P, Dorbolo S, Hari-Babu, N, Ntasis A, Cardwell D A and Campbell A M 2003 *IEEE Trans. Appl. Supercond.* **13** 3746-3749

[32] Vanderbemden P, Hong Z, Coombs T A, Denis S, Ausloos M, Schwartz J, Rutel I B, Hari Babu N, Cardwell D A and Campbell A M 2007 *Phys. Rev. B* **75** 174515

[33] Ogawa J, Iwamoto M, Yamagishi K, Tsukamoto O, Murakami M and Tomita M 2003 *Physica C* 386 26

[34] Fagnard J F, Kirsch S, Morita M, Teshima H, Vanderheyden B and Vanderbemden P 2015 *Physica C* **512** 42

[35] LeBlanc M A R, Celebi S and Rezeq M 2001 *Physica C*.**361** 251–259

[36] Baghdadi M, Ruiz H S and Coombs T A 2014 *Appl. Phys. Lett.* **104** 232602

[37] Funaki K and Yamafuji K 1982 *Jpn. J. Appl. Phys.* **21** 299

[38] Park S J and Kouvel J S 1993 *Phys. Rev. B* **48** 13 995–13 997

[39] Luzuriaga J, Badia-Majos A, Nieva G, Giordano J L, Lopez C, Serquis A and Serrano G 2009 *Supercond. Sci. Technol.* **22** 015021

[40] Clem J R, Weigand M, Durrel J H and Campbell A M 2011 *Supercond. Sci. Technol.* **24** 062002

[41] Egan R, Philippe M, Wera L, Fagnard J F, Vanderheyden B, Dennis A, Shi Y, Cardwell D A and Vanderbemden P 2015 *Rev. Sci. Instrum.* **86** 025107

[42] Dular P and Geuzaine C, GetDP Reference Manual: The Documentation for GetDP, a General Environment for the Treatment of Discrete Problems (2006) http://www.geuz.org/getdp

[43] Dular P 2001 Dual magnetodynamic finite element formulations with natural definitions of global quantities for electric circuit coupling *Scientific Computing in Electrical Engineering*, vol 18 (Berlin: Springer) 367–77

[44] Lousberg G P, Ausloos M, Geuzaine C, Dular P, Vanderbemden P and Vanderheyden B 2009 *Supercond. Sci. Technol.* **22** 055005

[45] Campbell A M 2011 J. *Supercond. Nov. Magn.* **24** 27–33

[46] Brandt E H 1998 *Phys. Rev. B* **58** 6506-6522

[47] Brandt E H 1996 *Phys. Rev. B* **54** 4246-4264

[48] Chen I G, Liu J, Weinstein R and Lau K 1992 *J. Appl. Phys.* **72** 1013–20

[49] Lousberg G P, Fagnard J F, Haanappel E, Chaud X, Ausloos M, Vanderheyden B and Vanderbemden P 2009 *Supercond. Sci. Technol.* **22** 125026

[50] Vanderbemden P, Molenberg I, Simeonova, P and Lovchinov V 2014 *J. Phys.: Confer. Ser.* **558** 012016